STATCOM Integration into a DFIG-based Wind Park for Reactive Power Compensation and its Impact on Wind Park High Voltage Ride-Through Capability

U. Karaagac, I. Kocar, J. Mahseredjian, L. Cai, Z. Javid

Abstract **– This paper presents static synchronous compensator (STATCOM) integration into a doubly-fed induction generator (DFIG) based wind park (WP), analyses the impact of STATCOM on the WP high voltage ride-through (HVRT) capability, and proposes a transient function for the STATCOM to improve the WP HVRT capability. An actual WP is adopted as a test system. The STATCOM size is selected considering the grid code requirement for power factor control, and various wind turbine (WT) and medium voltage (MV) feeder outage scenarios. The WP HVRT capability is assessed with electromagnetic transient (EMT) simulations by analyzing the responses to a parametric voltage waveform. The external system is represented by a Thevenin equivalent. The pre-described voltage waveforms are applied to the Thevenin source in order to assess the conformity of the HVRT capability to Hydro-Quebec specifications. The WP simulation model includes all details regarding collector grid and overvoltage protection. The simulation results demonstrate that, STATCOM usage provides a noticeable improvement in HVRT capability of the WP, especially with the proposed transient function.**

Keywords: **doubly-fed induction generator (DFIG), high voltage ride-through (HVRT), reactive power compensation, static synchronous compensator (STATCOM), wind park**

I. Introduction

The increase of wind power penetration has been forcing the transmission system operators (TSOs) to tighten their grid connection requirements in order to integrate the wind power generation without affecting the quality and stability of the grid. These connection requirements, called grid codes, include voltage regulation, power factor control, low voltage ride through (LVRT) and high voltage ride-through (HVRT) [1], [2].

The available reactive power at the point of interconnection (POI) is usually much less than the specified wind turbine (WT) capacity due to the reactive power losses at the WT transformers, the medium voltage (MV) collector grid and the wind park (WP) transformers. Therefore, reactive power compensation (RPC) may be required to fulfill the grid code requirement for the power factor control.

RPC has been traditionally handled with static VAR compensators (SVCs) [3]. However, when high dynamic performance is required, RPC must be handled with faster devices such as static synchronous compensator (STATCOM). Moreover, the compensation of SVCs depend on the voltage at POI while the compensation of the STATCOM is independent of that voltage [4].

The application of RPC device (STATCOM or SVC) to a DFIG based WP and its impact on LVRT capability has been reported in [5]-[9]. However, those researches have the several drawbacks, such as

- In [6]-[8], the considered DFIG based WP is obtained by scaling up a WT model to desired power level without taking the WP controller (WPC) into account. Hence, there is no coordination between the RPC device and WP.
- The WP voltage/reactive power control scheme in [9] includes a WPC that produces reactive power reference signal for the WTs. Hence, the WT outer control in [9] uses an automatic reactive power regulator (AQR) for actuating the WT reactive current. On the other hand, using automatic voltage regulator (AVR) for actuating the reactive current provides faster response. Moreover, WPC tuning becomes easier as the system dependency on the short circuit ratio (SCR) is reduced compared to a WP with an AQR at WTs [5]. Therefore, the WP voltage/reactive power control scheme in [9] is not expected to be common [10].
- The selection of the STATCOM size is not clear in [6]-[9] and quite large when the WP size is considered.
- The WP is represented with an aggregated WT and equivalent collector grid model in [5]-[9]. Hence, WT and MV feeder outage scenarios cannot be properly represented in simulations and potential partial trip scenarios cannot be identified.

Due to the reasons above, those researches need some refinements, extensions, and adaptations to study the impact of RPC devices on LVRT capability. Recent literature also does not contain any detailed study on HVRT capability of WPs and the impact of RPC devices on it. WPs may be subject to overvoltages that can occur during unbalance faults or following fault clearance, loss of large loads and switching on capacitor banks. The resulting overvoltages may have different magnitudes and durations, depending on the disturbance scenario. The HVRT behavior of the WTs is just an emerging issue [11], [12].

U. Karaagac and Z. Javid are with the Dept. of Electrical Engineering, The Hong Kong Polytechnic University, Hong Kong
I. Kocar and J. Mahseredjian are with the Dept. of Electrical Engineering, Polytechnique Montréal, Montréal, QC, Canada (i.kocar@polymtl.ca)
L. Cai is with the Institute for Electrical Power Engineering, University of Rostock, Rostock, Germany

Paper submitted to the International Conference on Power Systems Transients (IPST2021) in Belo Horizonte, Brazil June 6-10, 2021.

This paper presents an HVRT capability assessment study for an actual DFIG-based WP. The study is performed using detailed electromagnetic transient (EMT) model of the WP. The simulations consider various WT and MV feeder outage scenarios as well as STATCOM usage for RPC. This paper also proposes a transient function for the STATCOM to improve the HVRT capability of the WP. The simulations are performed using EMTP-RV [13]. The contributions of this paper are summarized below:

- The first demonstration of STATCOM integration study into a DFIG-based WP that considers industry level application,
- The first detailed research on STATCOM impact on HVRT capability of a DFIG-based WP,
- A transient function for STATCOM control to improve the WP HVRT capability.

The first part of this paper presents the WP under study. STATCOM integration and the proposed transient function is presented in the second part. The third part presents the calculation of the required RPC for the considered WP. The last part presents the HVRT capability simulation results.

II. System under Study

Simplified single-line diagram of the wind park is given in Fig.1. The wind park collector grid is composed of three radial 34.5 kV feeders and connected to 120 kV grid through a 120 MVA step-up transformer. The collector grid feeders F1, F2 and F3 contain 18, 7 and 15 DFIG-type WTs, respectively. Each WT has 2 MW rating and a reactive power capability range of -0.8/+0.9 MVAR (inductive/capacitive) at LV side of transformer. The WP transformer has an on-load-tap-changer (OLTC) to keep the 34.5 kV collector bus voltage at its nominal value. Depending on the selection of the function, either reactive power, voltage or power factor at POI (see Fig.1) is controlled by a central wind park controller (WPC) located at the wind park substation. Reader should refer to [14] for the WP details.

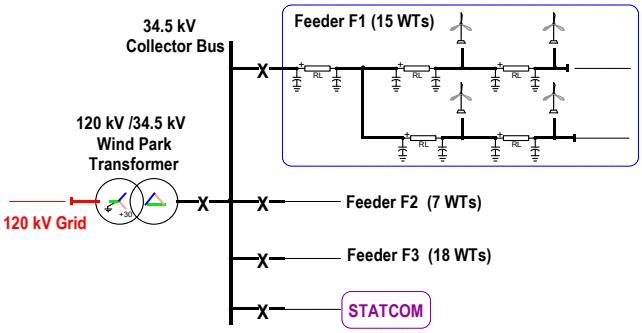

Fig. 1. Simplified single-line diagram of the considered wind park

A. Reactive Power Control in Wind Parks

The WP reactive power control is based on the secondary voltage control concept [5],[10],[15]. At primary level, WT controller (WTC) monitors and controls its own positive sequence terminal voltage (V_{dfig}) with a proportional voltage regulator. At secondary level, WPC monitors the reactive power at POI (Q_{POI}) and controls it by modifying the WTC reference voltage values ($V'_{dfig} = 1 + \Delta V'_{dfig}$) via a proportional-integral (PI) reactive power regulator while operating under reactive power control function (Q-control in Fig.2). In Fig.2 and henceforward, all variables are in pu and primed variables are used to indicate the reference values transmitted from controllers.

When WPC is operating under voltage control (V-control) function, the reactive power reference (Q'_{POI}) of the PI reactive power regulator is calculated by an outer proportional voltage control as shown in Fig.2. Although not shown in Fig.2, the WPC also contains a power factor control (PF-control) function where Q'_{POI} is calculated using the active power at POI (P_{POI}) and the desired power factor at POI (PF'_{POI}). This paper considers the WFC operating under V-control. Reader should refer to [16], for details.

B. Doubly-Fed Induction Generator Wind Turbines

In WTs with DFIG, the stator of the induction generator is directly connected to the grid and the wound rotor is connected to the grid through an ac-dc-ac converter system as shown in Fig.3. The ac-dc-ac converter system consists of two voltage source converters: rotor side converter (RSC) and grid side converter (GSC). A line inductor and shunt harmonic ac filters are used at the GSC to improve power quality (not shown in Fig.3). A crowbar is used to protect the RSC against overcurrent and the dc capacitor against overvoltage. To avoid the crowbar ignition during faults, dc resistive chopper is used to limit the dc voltage.

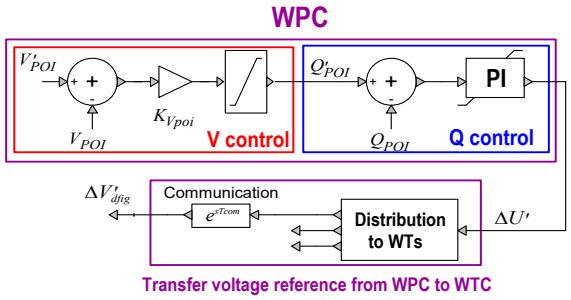

Fig. 2. Reactive power / voltage control at the POI

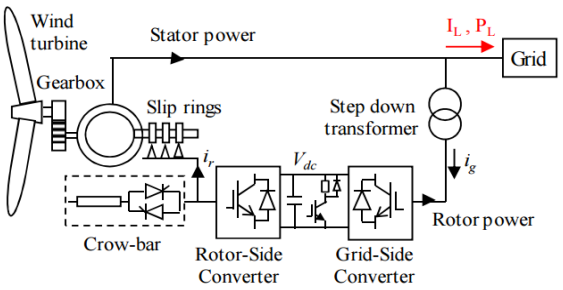

Fig. 3. Schematic diagram of DFIG WT

The control of the DFIG is achieved by controlling the RSC and GSC utilizing vector control techniques. The RSC controls the DFIG positive sequence terminal voltage (V_{dfig}) and the active power output of the DFIG (P_{dfig}) determined by the maximum power point tracking (MPPT) function. On the other hand, the GSC is used to maintain the dc bus voltage. During normal operation, the RSC controller gives the priority to the active currents and GSC operates at unity power factor. Reader should refer to [16] for details.

C. Fault-Ride-Through (FRT) Function

The WTs are equipped with an FRT function to fulfill the grid code requirements regarding voltage support such as the one shown in Fig.4. The FRT function is activated when the voltage deviation $|1 - V_{dfig}|$ exceeds the pre-defined value V_{FRT-ON} and deactivated when the voltage deviation reduces below the pre-defined value $V_{FRT-OFF}$ after a pre-specified release time t_{FRT}. When the FRT function is active, the DFIG injects reactive current proportionally to voltage deviation from 1pu (see Fig.4).

During FRT operation the RSC controller gives the priority to the reactive current. The GSC also injects reactive currents during faults when the RSC reactive current contribution is not sufficient to satisfy the grid code requirement due to the reactive current absorbed by the IG. Reader should refer to [16] for details.

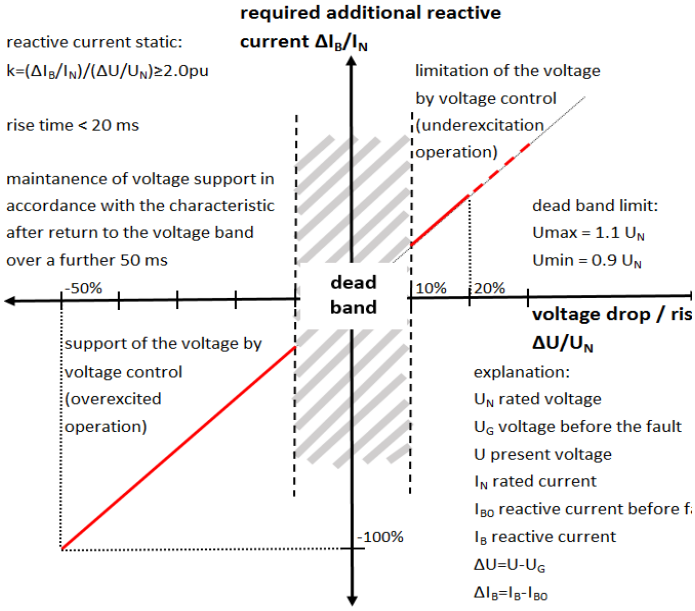

Fig. 4. WT reactive output current during voltage disturbances [17]-[18].

It should be also noted that, when a severe voltage sag occurs at POI (due to a fault), the PI regulator output of the WPC ($\Delta U'$ in Fig.2) is kept constant by blocking the input ($Q'_{POI} - Q_{POI}$) to avoid overvoltage following the fault removal.

III. Static Synchronous Compensator (STATCOM)

The considered STATCOM hardware (see Fig.5) consists of a two-level PWM-based converter connected to a capacitor which carries the dc voltage. A line inductor and shunt harmonic ac filters are used to improve power quality. The STATCOM is connected to grid through a coupling transformer.

Similar to DFIG, the STATCOM control is achieved utilizing vector control techniques. The outer controls (Q control and Vdc control) calculate the references for the reactive and active currents (i'_{react} and i'_{act}, respectively) based on reactive power demand from STATCOM and the pre-specified dc bus voltage. The inner control (current control) permits controlling the STATCOM ac voltage reference. The considered STATCOM allows short term overloading. Hence, the limits on current references are function of time and total converter current.

A. WPC and STATCOM Coordination

The coordination between WPC and STATCOM is achieved using the outer proportional voltage control of STATCOM to generate the reactive power reference value for the inner reactive power control of the WPC as shown in Fig.6. Following a sudden change in V_{POI}, the STATCOM is expected to provide either the reactive power mismatch ($Q'_{POI} - Q_{POI}$) or its maximum output (if $Q'_{POI} - Q_{POI}$ is larger than its capacity) as its response time is much faster compared to the reactive power controller of the WPC. As the contribution of WTs in Q_{POI} will increase in time, the reactive power generated by STATCOM will reduce and reach to zero if initial reactive power mismatch is less than the available reactive power reserve in WTs.

In Fig.6, the limit $f(t, I_{STATCOM})$ is a function of time and total converter current.

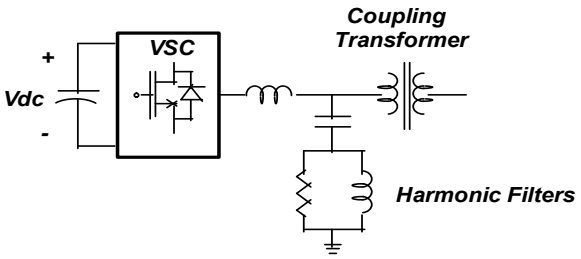

Fig. 5. Simplified circuit diagram of a STATCOM

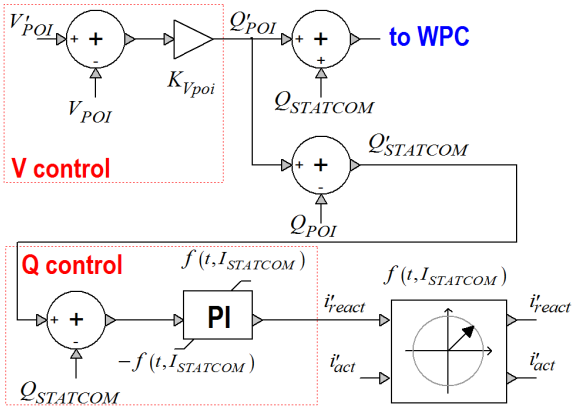

Fig. 6. STATCOM reactive power control

B. Linearized System Model and Parameter Tuning

Considering ideal decoupling, the simplified WP representation in Fig.7 and STATCOM representation in Fig.8 can be used for the analysis of reactive power control [5]. The measurement system (grid meter) is represented by a first order function with time constant T_m. The WP control include the delay associated to the sampling (T_S) process. The communication delays are ignored as $T_S = 100ms$. X_{GRID} is the HV grid impedance seen by the wind park and X_{WP} is the equivalent impedance between the DFIG terminal and POI. The DFIG and STATCOM is represented by a first order function with time constants τ_c and τ_S, respectively.

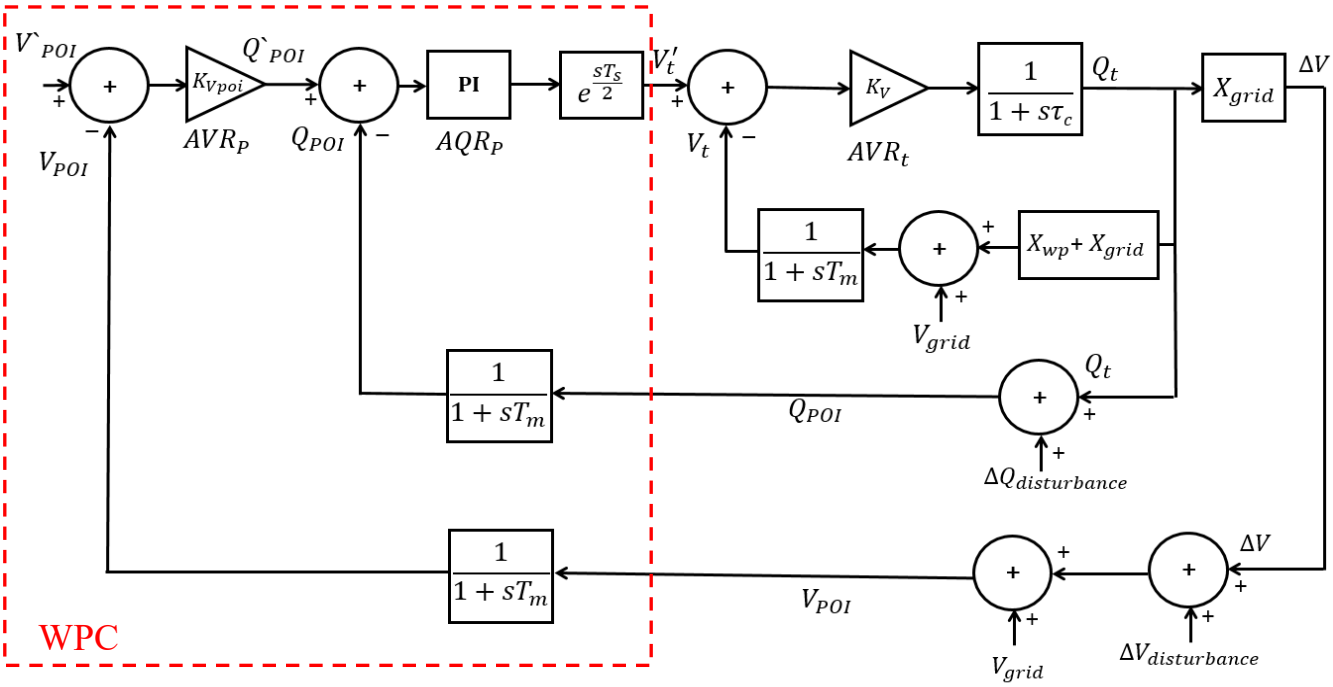

Fig. 7. Simplified representation of WP for the analysis of reactive power control.

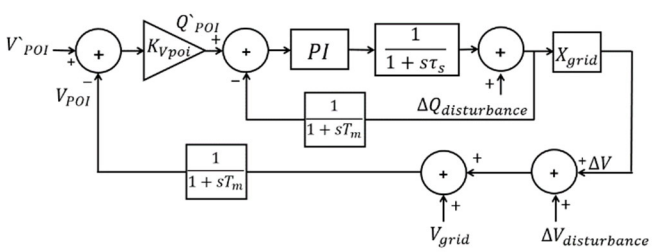

Fig. 8. Simplified representation of STATCOM for the analysis of reactive power control.

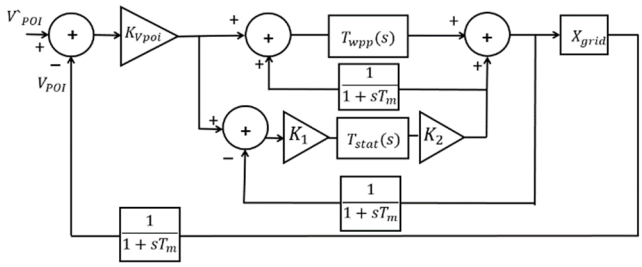

Fig.9. Simplified representation of WP after STATCOM integration

Fig.9 illustrates the simplified WP model after STATCOM integration. The transfer functions representing WP and STATCOM ($T_{wpp}(s)$ and $T_{stat}(s)$ in Fig.9) are given below:

$$T_{wpp}(s)=\frac{AQR_p\, e^{\left(\frac{sT_s}{2}\right)} K_V\left(1/(1+s\tau_c)\right)}{1+K_V\left(1/(1+s\tau_c)\right)(X_{wpp}+X_{grid})\left(1/(1+sT_m)\right)} \quad (1)$$

$$T_{stat}(s)=\frac{AQR_{stat}\ \left(1/(1+s\tau_S)\right)}{1+AQR_{stat}\ \left(1/(1+s\tau_S)\right)\left(1/(1+sT_m)\right)} \quad (2)$$

$K_1 = K_2^{-1} = S_{wp}/S_{stat}$ where S_{wp} and S_{stat} are the base powers for the WP and STATCOM, respectively.

The PI parameters of the STATCOM reactive power regulator (AQR_{stat}) is adjusted using the internal model control (IMC) technique [19] considering the STATCOM rise time. The grid meter is ignored.

$$K_P = BW \times \tau_S$$
$$K_I = BW \quad (3)$$

where BW is the bandwidth, and bandwidth - rise time (τ_{rise}) relation of a first-order system is $BW = \ln(9)/\tau_{rise}$.

To improve the HVRT capability of the WP, the rise time of the STATCOM is decreased from τ_{rise} = 250 ms (typical manufacturer data). The stability assessment is performed using the simplified WP model shown in Fig.9. 10, 20 and 30 WT outage scenarios are considered in addition to the no WT outage scenario (base case). X_{GRID}, X_{WP}, K_1 and K_2 are modified in the simplified model considering the WT outage scenario. The system stability margins remain at acceptable level for the STATCOM rise time τ_{rise} = 25 ms (i.e., phase margin (PM) larger than 30 degrees and the gain margin (GM) larger than 2 dB). It should be noted that, especially the PM decreases with the decrease in the number of WTs in service inside the WP for the same STATCOM rise time.

C. Proposed Transient Function

The impact of STATCOM on LVRT and HVRT performance of the WP strongly depends on the reactive power control loop PI regulator parameters (see Fig.6). Those parameters should be set to enable fast (and stable) response in order to improve the LVRT and HVRT capabilities of the WP as explained above. However, the STATCOM may not exhibit the desired performance when the overvoltage condition occurs following a voltage dip as the accumulated value at the integral of the PI regulator during voltage dip

prevents immediate STATCOM response to the overvoltage.

This paper proposes a transient function that activates a proportional voltage control following a significant voltage deviation at MV side of the STATCOM transformer (V_{MV}) as shown in Fig.10. It should be noted that V_{MV} is kept around 1 pu by the WP transformer OLTC. The block "activate V regulator" activates the voltage control when the voltage deviation $|1 - V_{MV}|$ exceeds the pre-defined value V_{ON} and deactivated when the voltage deviation reduces below the pre-defined value V_{OFF} after a pre-specified release time t_{RT}.

IV. Reactive Power Compensation Requirement

The WP should be capable of operating over a power factor range shown in Fig.11 [18]. By ignoring the voltage drop in the WP and the currents on the shunt branches, the reactive power output of the WP at POI can be approximated by:

$$Q_{POI} = Q_{WT} - X_S\, I_{POI}^2 - \left(\frac{1}{X_m} - Y_{CG}\right) V_{POI}^2 + Q_{COMP} \quad (4)$$

where Q_{WT} is the total reactive power supplied by the WTs; I_{POI} is the total current output of the WP at POI; X_S is the equivalent series reactance of the cables, lines and transformers; X_m is the equivalent magnetizing reactance of the transformers; Y_{CG} equivalent shunt admittance of the lines and cables; Q_{COMP} is the injected reactive power by the RPC system (if exists).

The required size of the RPC system is found as $-4.85\ MVAR \leq Q_{COMP} \leq 1.65\ MVAR$ using equation (4) and considering various WT and MV feeder outage scenarios. The STATCOM size is selected as 5 MVAR (2 x 2.5 MVAR).

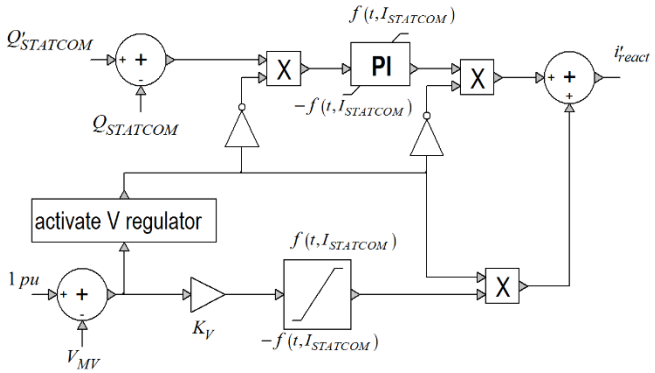

Fig. 10. Proposed STATCOM outer control (reactive current channel)

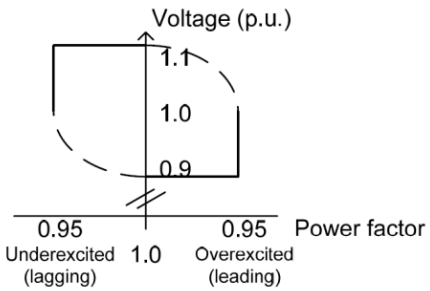

Fig. 11. Wind park power factor capability versus voltage at POI [18]

V. EMT Simulations

The external system is represented by a Thevenin equivalent where the source is a pre-described voltage waveform that imitates an overvoltage condition following a voltage dip. The aforementioned overvoltage conditions occur following a 2.5-cycle 50% voltage dip. It should be noted that, according to the analysis of the data from the transient recorders, a severe overvoltage may occur during the fault recovery period. The utilized parametric voltage waveform is described as below:

$$\begin{aligned}
&t < 0.96,\ V_a = V\cos(\omega t)\\
&0.96 \leq t < 1,\ V_a = 0.5\,V\cos(\omega t)\\
&1 \leq t < 1.033,\ V_a = 1.4\,V\cos(\omega t) + \sum_{k=1,3,5,7} h_k\, V\cos(k\,\omega t)\\
&1.033 \leq t < 1.1,\ V_a = 1.4\,V\cos(\omega t)\\
&1.1 \leq t,\ V_a = V\cos(\omega t)
\end{aligned} \quad (5)$$

The objective of these simulations is to determine to maximum power-frequency (60 Hz) overvoltage that can be applied to the system for the first two cycles followed by a 4-cycle 1.4 pu overvoltage without any WT trips. It should be noted that, the parametric waveform in (5) also enables to test the WP HVRT capability for various harmonic overvoltage conditions. For this purpose, various 3rd, 5th and 7th harmonic voltages are added to the 1.4 pu power-frequency overvoltage during the first two-cycle period. This paper only considers power-frequency overvoltages due to space limitations.

The collector grid cables and lines are represented with their coupled pi sections. All transformer models include magnetic saturation. The surge arresters connected to the DFIG and WP transformers are also included. A generic 2 MW, 60 Hz DFIG-type WT model is used. The DFIG converters are modeled with their average value models (AVMs) [20],[21]. Reader should refer to [8] for details.

The generic STATCOM model of the EMTP library is used after making necessary modifications for the coordination with WPC as well as the modifications for the proposed transient function and the short term overloading capability. Similar to DFIG, the STATCOM converter is also modeled using AVM.

A. Simulation Scenarios

The overvoltage scenarios are presented in Table I, where h1 is the additional power-frequency overvoltage term defined in (5). The WT and MV feeder outage scenarios are presented in Table II. Those outages are expected to have a significant impact on HVRT capability due to reduced reactive power capacity in the WP. The STATCOM scenarios are presented in Table III. STATCOM1 is the one with τ_{rise} = 250 ms (typical manufacturer data)

B. Simulation Results

The maximum values phase rms voltages at MV collector bus are presented in Fig.12 for the simulation scenarios F0-G1-NONE - F0-G10-NONE. The maximum phase rms voltages at DFIG terminals are lower than the maximum phase rms voltages at MV collector bus. It should be noted that, the DFIG overvoltage protection operates when the

maximum of phase rms voltages at DFIG terminals exceeds the threshold value of 1.3 pu. None of the WTs trip in the scenarios presented in Fig.12. The total reactive power delivered to the MV collector bus is presented in Fig.13.

TABLE I. POWER FREQUENCY OVERVOLTAGES IN HVRT TESTS

Scenario	*F0*	*F1*	*F2*	*F3*	*F4*	*F5*	*F6*
h1	0	0.025	0.05	0.075	0.1	0.15	0.2

TABLE II. WIND TURBINE / MV FEEDER OUTAGE SCENARIOS

Scenario	*# of WT outages*	*WT / Feeder outage detail*
G1	0	-
G2	7	F2 out
G3	10	4 WT on F1, 2 WT on F2, 4WT on F3 out
G4	15	F1 out
G5	18	F3 out
G6	20	7 WT on F1, 4 WT on F2, 9WT on F3 out
G7	22	F1 and F2 out
G8	25	F2 and F3 out
G9	30	11 WT on F1, 5 WT on F2, 14WT on F3 out
G10	33	F1 and F3 out

TABLE III. STATCOM SCENARIOS

Scenario	*STATCOM*
NONE	No reactive power compensation
STATCOM1	5 MVAR slow response STATCOM (τ_{rise} = 250 ms)
STATCOM2	5 MVAR fast response STATCOM (τ_{rise} = 25 ms)
STATCOM3	STATCOM1 with proposed transient function

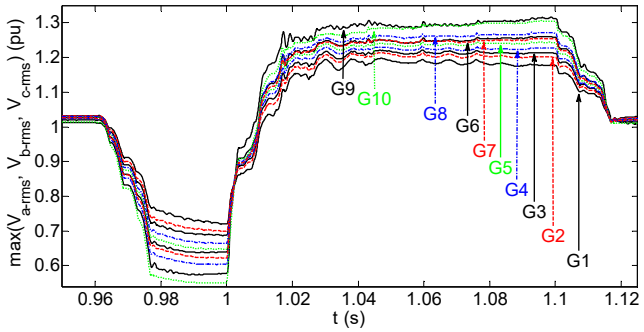

Fig. 12. Maximum of phase rms voltages at MV collector bus, F0, NONE

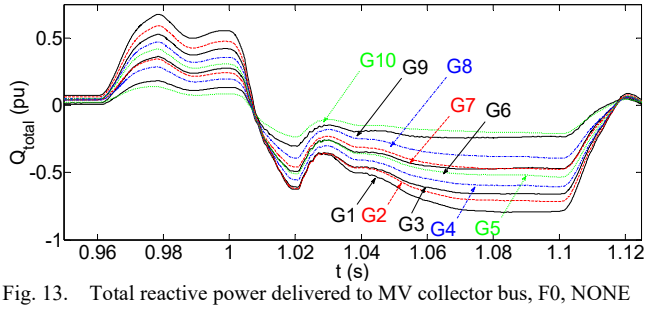

Fig. 13. Total reactive power delivered to MV collector bus, F0, NONE

Fig.12 and Fig.13 demonstrate not only the impact of WT outages on HVRT capability, but also the impact of outages in collector grid. The impact of outages in collector grid is apparent in G9 and G10. The collector grid voltage profile is higher in G9 compared to G10 although the number of WT outages is higher in G10. However, in G10, the collector grid produces less reactive power compared to G9 due to the outages in collector grid MV feeders. It should be noted that, the situation is similar in simulation scenarios G6 and G7. The HVRT capability test results are summarized in Table IV for no RPC scenarios.

TABLE IV. HVRT CAPABILITY TEST RESULTS - NONE

Scenarios	*F1 - F3*	*F4*	*F5*	*F6*
G1 - G3	No Trip	No Trip	No Trip	No Trip
G4 - G7	No Trip	No Trip	No Trip	***All Trip***
G8	No Trip	No Trip	***All Trip***	***All Trip***
G9 - G10	No Trip	***All Trip***	***All Trip***	***All Trip***

The maximum of phase rms voltages for DFIG-A5 is presented in Fig.14 for the simulation scenarios F4-G9-NONE - F4-G9-STATCOM3. The voltages at DFIG-A5 terminals are the highest when compared to other DFIGs. As seen in Fig.14, STATCOM1 has negative impact on HVRT capability of the wind park due to its slow response. However, this negative impact is not noticeable as HVRT capability test results for STATCOM1 is same with the Table IV.

When the STATCOM1 reactive control loop parameters are tuned for fast response (STATCOM2) or it is equipped with the proposed transient function (STATCOM3), it provides a noticeable improvement in HVRT capability of the wind park. On the other hand, even tuned for fast response, STATCOM2 exhibits poor response compared to STATCOM3 (see Fig.14 and Fig.15). The accumulated value in the integral of the PI regulator during voltage sag prevents immediate response of STATCOM2 to the overvoltage. This is also confirmed in Table V and Table VI. These tables summarize the HVRT capability test results for STATCOM2 and STATCOM3, respectively.

It should be noted that, further decrease in STATCOM rise time (such as τ_{rise} = 20 ms) results a noticeable decrease in PM (21 degrees). Although the system remains stable, the reactive power output of the STATCOM makes oscillations following the sudden voltage changes and results inferior HVRT capability compared to the STATCOM with τ_{rise} = 25 ms.

It should be emphasized that, the simplified model shown in Fig.9 is valid for small perturbations. This research focuses on the transient response to a large disturbance which causes activation of nonlinearities (such as saturation of transformers, saturation of converters, overvoltage protection, etc.). Hence, representative EMT simulations are essential to conclude on the performance of STATCOM2 for different rise time settings. If further improvement was possible in STATCOM2 response (such as τ_{rise} = 20 ms), its performance would be still poor compared to STATCOM3 due to the accumulated value in the integral of the PI regulator during the voltage sag.

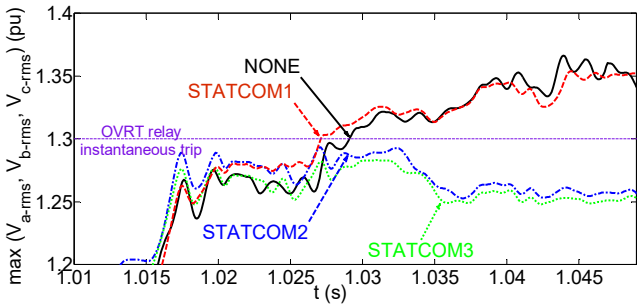

Fig. 14. Maximum of the phase rms voltages at DFIG-A5, G9, F4

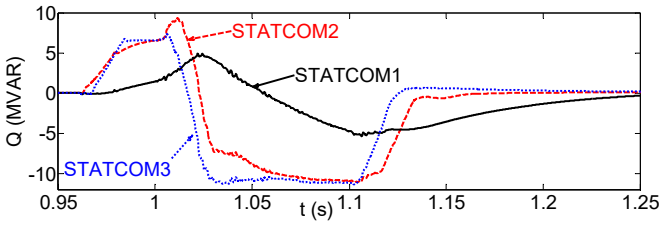

Fig. 15. Reactive Power Injected by the STATCOM, G9, F4

TABLE V. HVRT CAPABILITY TEST RESULTS - STATCOM2

Scenarios	*F1 - F4*	*F5*	*F6*
G1 - G4	No Trip	No Trip	No Trip
G5	No Trip	No Trip	***Partial Trip****
G6 - G8	No Trip	No Trip	***All Trip***
G9 - G10	No Trip	***All Trip***	***All Trip***

* All WTs trip on Feeder F2 (7 WTs)

TABLE VI. HVRT CAPABILITY TEST RESULTS - STATCOM3

Scenarios	*F1 - F4*	*F5*	*F6*
G1 - G5	No Trip	No Trip	No Trip
G6 - G8	No Trip	No Trip	***All Trip***
G9 - G10	No Trip	***All Trip***	***All Trip***

VI. CONCLUSION

This paper presented STATCOM integration into a DFIG based WP for the power factor control, analyzed its impact on the WP HVRT capability and proposed a transient function for the STATCOM to improve the WP HVRT capability. An actual WP was adopted as a test system and a detailed EMT model was utilized that contains all details regarding collector grid and overvoltage protection.

STATCOM provides a noticeable improvement in HVRT capability of the WP when its reactive control loop parameters are tuned for fast response (STATCOM2) or the slow response one (STATCOM1) is equipped with the proposed transient function (STATCOM3). The proposed transient function simply blocks the PI reactive power regulator and activates a proportional voltage regulator when there is a large voltage sag or swell in the MV collector bus. Even tuned for fast response, STATCOM2 exhibits poor response compared to STATCOM3 as the accumulated value in the integral of the PI reactive power regulator during voltage sag prevents immediate response of STATCOM2. Moreover, the fast response of STATCOM2 comes at the expense of reduced stability margins. It should be also noted that, STATCOM's fast response may not be desirable by the TSO as it (the entire WP as well) will be a part of transmission system centralized voltage control system.

The wind park has enough HVRT capability even for WT outages more than 75% of its total capacity. Therefore, SVC usage can be preferred for reactive power compensation (due to its cost), although it is not expected to provide any improvement in the WP HVRT capability.

VII. ACKNOWLEDGEMENTS

This work was partially supported by the Department of Electrical Engineering at The Hong Kong Polytechnic University through the Start-up Fund Research Project under Grant 1-ZVLU and partially supported by German Federal Ministry for the Environment, Nature Conservation, Building and Nuclear Safety (grant code: 032529).

VIII. REFERENCES

[1] Wind Plant Collector Design WG, "Reactive Power Compensation for Wind Power Plants," *IEEE PES General Meeting*, Calgary, Canada, July 2009.

[2] M. Tsili and S. Papathanassiou, "A review of grid code technical requirements for wind farms," *IET Renew. Power Generation*, vol. 3, no. 3, pp.308 -332, 2009.

[3] The FACTS Terms and Definitions Task Force of the FACTS Working Group of the DC and FACTS Subcommittee, "Proposed terms and definitions for Flexible AC Transmission System (FACTS)", *IEEE Trans. on Power Delivery*, Vol. 12, No. 4, pp. 1848-1853, Oct. 1997.

[4] L. Gyugyi, "Solid-state synchronous voltage sources for dynamic compensation and real-time control of AC transmission lines," *IEEE Emerging Practices in Technology*, 1993.

[5] J. M. Garcia, "Voltage control in wind power plants with doubly fed generators," Ph.D. dissertation, Aalborg Univ., Denmark, Sep. 2010.

[6] W. Qiao, G. K. Venayagamoorthy and R. G. Harley, "Real-Time Implementation of a STATCOM on a Wind Farm Equipped With Doubly Fed Induction Generators," in IEEE Transactions on Industry Applications, vol. 45, no. 1, pp. 98-107, 2009.

[7] M.K. Döşoğlu, A.B. Arsoy, U. Güvenç, "Application of STATCOM-supercapacitor for low-voltage ride-through capability in DFIG-based wind farm", *Neural Comput. Appl.*, Vol. 28, Iss. 9, pp. 2665-2674, 2017.

[8] D H. Rezaie, M. H. Kazemi-Rahbar, "Enhancing voltage stability and LVRT capability of a wind-integrated power system using a fuzzy-based SVC", Engineering Science and Technology, an International Journal, Vol. 22, Iss. 3, pp. 827-839, 2019.

[9] Qi, J., W. Zhao, and X. Bian, "Comparative Study of SVC and STATCOM Reactive Power Compensation for Prosumer Microgrids with DFIG-Based Wind Farm Integration," *IEEE Access*, vol. 8, pp. 209878-209885, 2020.

[10] U. Karaagac, J. Mahseredjian, R. Gagnon, H. Gras, H. Saad, L. Cai, I. Kocar, A. Haddadi, E. Farantatos, S. Bu, K. W. Chan, L. Wang, "A Generic EMT-type Simulation Model for Wind Parks with Permanent Magnet Synchronous Generator Full Size Converter Wind Turbines," *IEEE Power Energy Technol. Syst.* J., vol. 6, no. 3, pp. 131-141, Sept. 2019.

[11] Feltes, S. Engelhardt, J. Kretschmann, J. Fortmann, and F. K. I. Erlich, "High voltage ride-through of DFIG-based wind turbines," *IEEE PES General Meeting*, Pittsburgh, USA, July 20-24, 2008.

[12] M. Mohseni, M. Masoum, and S. Islam, "Low and high voltage ride-through of DFIG wind turbines using hybrid current controlled converters," *Electric Power Systems Research*, vol. 7, pp. 1456-1465, 2011.

[13] J. Mahseredjian, S. Dennetière, L. Dubé, B. Khodabakhchian and L. Gérin-Lajoie: "On a new approach for the simulation of transients in power systems," *Electric Power Systems Research*, vol. 77, Issue 11, pp. 1514-1520, Sep. 2007

[14] U. Karaagac, J. Mahseredjian and L. Cai, "Ferroresonance Conditions in Wind Parks," *Electric Power Systems Research*, vol. 138, pp. 41-49, Sep. 2016.

[15] M. Ghafouri, U. Karaagac, J. Mahseredjian and H. Karimi, "SSCI Damping Controller Design for Series Compensated DFIG based

Wind Parks Considering Implementation Challenges" *IEEE Trans. Power Syst.*, vol. 34, no. 4, pp. 2644-2653, July 2019.

[16] U. Karaagac, J. Mahseredjian, H. Gras, H. Saad, J. Peralta and L. D. Bellomo, "Simulation Models for Wind Parks with Variable Speed Wind Turbines in EMTP-RV", research report, Polytechnique Montréal, Dec. 2016.

[17] "Grid code - high and extra high voltage," E.ON Netz GmbH, Bayreuth, Germany, April 2006.

[18] "Transmission provider technical requirements for the connection of power plants to the Hydro-Quebec transmission system," Direction Planification des actifs, February 2009.

[19] Roffel B and Betlem BH, "Advanced Practical Process Control," Springer-Verlag, Berlin, 2004.

[20] J. Morren, S. W. H. de Haan, P. Bauer, J. Pierik, and J. Bozelie, "Comparison of complete and reduced models of a wind turbine with Doubly-fed Induction Generator," *10th Eur. Conf. Power Electron. Appl.*, Toulouse, France, Sep. 2003, pp. 1–10.

[21] J. G. Slootweg, H. Polinder, and W. L. Kling, "Representing wind turbine electrical generating systems in fundamental frequency simulations," *IEEE Trans. Energy Convers.*, vol. 18, no. 4, pp. 516–524, Dec.2003.